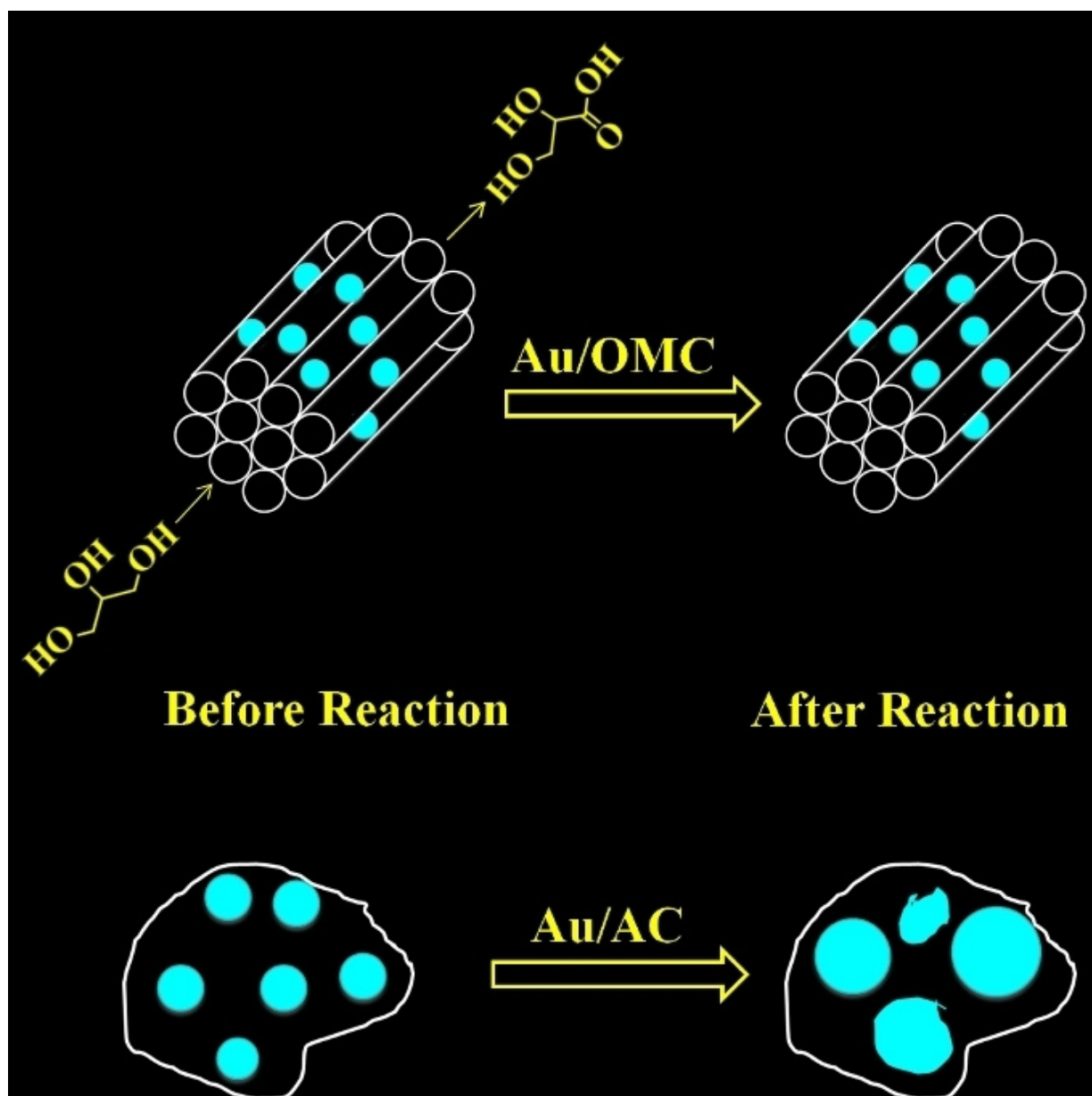


The Enhanced Catalytic Performance and Stability of Ordered Mesoporous Carbon Supported Nano-gold with High Structural Integrity for Glycerol Oxidation

Palle R. Murthy^[a] and Parasuraman Selvam^{*[a, b, c]}

Dedicated to Dr. M. Lakshmi Kantam on the occasion of her 63rd birthday

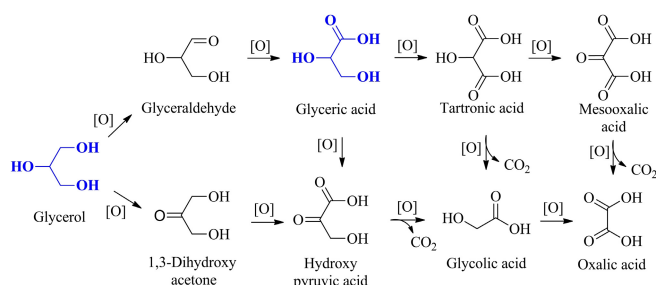


Abstract: Ordered mesoporous carbon (OMC) supported gold nanoparticles of size 3–4 nm having uniform dispersion were synthesized by sol-immobilization method. OMCs such as CMK-3 and NCCR-56 with high surface area and uniform pore size were obtained, respectively, using ordered mesoporous silicas such as SBA-15 and IITM-56 as hard templates, respectively. The resulting OMC supported monodispersed nano-gold, i. e., Au/CMK-3 and Au/NCCR-56, exhibited excellent performance as mild-oxidizing catalysts for oxidation of glycerol with high hydrothermal stability. Further, unlike activated carbon supported nano-gold catalysts (Au/AC), the OMC supported nano-gold catalysts, i. e., Au/CMK-3 and Au/NCCR-56, show no aggregation of active species even after recycling. Thus, in the case of Au/CMK-3 and Au/NCCR-56, both the fresh and regenerated catalysts showed excellent performance for the chosen reaction owing to an enhanced textural integrity of the catalysts and that with remarkable selectivity towards glyceric acid. The significance of the OMC supports in maintaining the dispersion of gold nanoparticles is explicit from this study, and that the activity of Au/AC catalyst is considerably decreased (~50%) upon recycling as a result of agglomeration of the active gold nanoparticles over the disordered amorphous carbon matrix.

Keywords: Glycerol oxidation, Glyceric acid, Nano-Gold, Ordered mesoporous carbon, CMK-3, Activated carbon.

1. Introduction

Supported gold catalysts are used in oxidation and hydrogenation reactions.^[1] They are predominantly employed in alcohol oxidation especially glycerol oxidation reaction (Scheme 1)^[2] as glycerol, a by-product of transesterification reaction in the production of bio-diesel, is one of the important bio-refinery feedstock.^[3] The glycerol availability will increase sharply due to an increase in bio-diesel



Scheme 1. Products obtained by the oxidation of glycerol.^[9]

[a] *Dr. P. R. Murthy, Prof. Dr. P. Selvam*
National Centre for Catalysis Research and Department of Chemistry
Indian Institute of Technology Madras
Chennai 600 036 (India)
E-mail: selvam@iitm.ac.in

[b] *Prof. Dr. P. Selvam*
School of Chemical Engineering and Analytical Science
The University of Manchester
Manchester M13 9PL (United Kingdom)

[c] *Prof. Dr. P. Selvam*
Department of Chemical and Process Engineering
University of Surrey, Guildford
Surrey GU2 7XH (United Kingdom)

production. Owing to the high functionality, glycerol can be used in synthesizing different value-added chemicals through oxidation, hydrogenolysis, dehydration, etherification, esterification, pyrolysis, polymerization, etc.^[4] Glyceric acid is one of the major oxidation products of glycerol and has extensive applications in variety of biological activities like liver stimulant and cholesterolytic activity, base material for functional surfactants and monomer for oligoesters or polymers.^[5] Therefore, it is important to control the oxidation process in order to obtain this valuable and desired product. Supported gold nanoparticles are showing promising results for glycerol oxidation compared to several other noble metal nanoparticles.^[6] Nano-gold exhibits superior activity for selective oxidation of organic molecules due to the higher fraction of surface atoms with low coordination numbers^[7] when compared to bulk gold which has filled d band and high activation energy barrier. In order to increase stability and avoid aggregation, gold nanoparticles are dispersed on high surface area carbon or metal oxide supports.^[8] Ordered porous carbon with uniform pore structure and high surface area is considered as most attractive support in view with its stability and chemical inertness.^[7a]

In general, ordered mesoporous carbons (OMC) are prepared by soft and hard-templating method, primarily using surfactant-templated silica frameworks^[10] and the process depends on the action of carbonizing carbon precursors inside the pores of silica. Specifically, OMC like CMK-1 and CMK-3 have been produced by carbonizing the organic precursor inside the pores of MCM-48 and SBA-15, respectively.^[5,7] In the case of noble metal nanoparticles supported on OMCs show profound applications in catalysis, electrochemistry and fine-chemical synthesis. In this regard, platinum supported on OMCs were widely studied for direct methanol fuel cell applications^[11] while gold supported on

OMCs were mostly used in organic transformations.^[12] In this context, we have synthesized OMCs such as CMK-3 and NCCR-56 using SBA-15 and IITM-56 as hard-templates, respectively. These OMCs were then employed as supports for gold nanoparticles, and the resulting supported nano-gold catalysts, viz., Au/CMK-3 and Au/NCCR-56, were utilized for glycerol oxidation reaction. The uniform pore size of the OMC supports are mainly responsible for stabilizing the nanoparticles and hence the recyclability of the catalyst is also examined. In addition, the efficiency of these catalysts was also evaluated in relation to the popularly known catalysts such as activated carbon supported gold catalysts, Au/AC.

2. Experimental

2.1. Starting Materials

The chemicals used in this study are of analytical grade: Pluronic P-123, Brij-56, tetraethyl orthosilicate (TEOS, 98.0%, Sigma Aldrich), methanol (99.9%), hydrofluoric acid (Merck) and sulphuric acid (98.0%, Merck), sodium tetrachloroaurate (III) dihydrate (99.0%, Sigma Aldrich) and activated carbon from SD fine chemicals, sodium borohydride (95.0%, SRL), tri-sodium citrate (99.0% SRL) and

polyvinyl alcohol (PVA, average MW 14,000, CDH), glycerol (99.5%, Rankem), glyceric acid (95.0%, Aldrich).

2.2. Synthesis of OMSs

SBA-15: Ordered mesoporous silica, SBA-15 was prepared by adding tetraethoxysilane (TEOS) into the hydrochloric acid solution of triblock co-polymer P123. The molar composition was 1 TEOS: 0.017 P123: 5.9 HCl: 193 H₂O. The mixture was stirred at 40 °C for 20 h, followed by hydrothermal treatment at 100 °C for 48 h. The solid product obtained was filtered and dried overnight at 80 °C followed by calcination at 550 °C for 6 h in the presence of air atmosphere.^[13]

IITM-56: The ordered mesoporous silicate, referred as IITM-56, was synthesized adopting a previously reported method.^[14] The molar gel composition was 1 TEOS: 0.15 Brij-56: 11.30 HCl: 119 H₂O. In a typical synthesis, 4.0 g of Brij 56 was added to 20 mL of water and the solution was stirred at 50 °C until a clear solution was obtained. Thereafter, 80 mL of 2 M HCl was added to the solution and further stirred for 2 h. Then, 8.3 g of (TEOS) was added and stirred at 50 °C for 24 h. The resulting mixture was transferred to an autoclave and hydrothermally treated at 100 °C for 24 h. Obtained precipitate was filtered, washed,



Dr. Palle Ramana Murthy obtained MSc degree in Chemistry from Andhra University, Visakhapatnam, India, and PhD in Catalysis from the Indian Institute of Technology (IIT) -Madras, Chennai, India. The research work presented here was carried out at the National Center for Catalysis Research (NCCR), IIT-Madras. His research interests include supported catalyst systems and their applications in biomass conversion and selective oxidation processes.



Prof. Dr. Parasuraman Selvam is currently Head, National Center for Catalysis Research, and Professor in the Department of Chemistry, IIT-Madras, Chennai, India; Adjunct Faculty, School of Chemical Engineering and Analytical Science, The University of Manchester, Manchester, U.K., and Department of Chemical and Process Engineering, University of Surrey, Guildford, U.K. Earlier, Prof. Selvam was a Faculty at IIT-Bombay, Mumbai, India, and Tohoku University, Sendai, Japan. He

was also a Visiting Associate Professor in the School of Chemical Engineering, The University of Queensland, Brisbane, Australia, and an Eminent International Visiting Professor in the School of Science and Health, Western Sydney University, Penrith, Australia. Prior to these, Prof. Selvam was a Post-Doctoral Research Associate in the Department of Condensed Matter Physics, and Laboratory of X-ray Crystallography, University of Geneva, Geneva, Switzerland. His research interests are in the areas of solid state and surface chemistry with an emphasis on nano-structured materials and their applications in heterogeneous catalysis as well as energy conversion, storage and environmental remediation processes. Prof. Selvam has filed about 20 patents and published over 300 original research papers in peer-reviewed journals and conference proceedings. <https://www.iitm.ac.in/info/fac/selvam>

dried at 60 °C for 6 h and calcined at 550 °C for 1 h in nitrogen followed by 5 h in air atmosphere at a heating rate of 1 °C/min in order to obtain surfactant free OMS, *i.e.*, IITM-56.

2.3. Synthesis of OMCs

CMK-3 and NCCR-56: Ordered mesoporous carbons CMK-3 and NCCR-56 were prepared as per the reported procedure.^[13a,15] Initially, IITM-56^[14] was added to an acidified sucrose solution obtained by dissolving suitable amount of sucrose and H₂SO₄ in water. The mixture was dried at 100 °C for 6 h followed by drying at 160 °C for 6 h. The impregnation step was repeated at this stage. Prior to impregnating sucrose solution, the silica template was dried in vacuum at 100 °C for 30 min. The dark black colored sample obtained was carbonized at 900 °C under nitrogen flow for 6 h with heating rate of 5 °C/min. The silica template was removed by dissolving in dil. HF. Similarly, CMK-3 was prepared using SBA-15 as hard template. The resulting carbon materials were washed with ethanol and dried at 120 °C for 6 h and systematically characterized by various analytical and spectroscopic techniques.

2.4. Preparation of Au/OMC and Au/AC

Gold nanoparticles were immobilized on carbons (OMC and AC) via the formation of a gold-sol and subsequent deposition of the sol onto the carbon support.^[16] Initially, PVA (2% *w/w*, 0.706 mL) was added to the NaAuCl₄·2H₂O (140 mL, 5 × 10⁻⁴ M) solution, which was subsequently reduced by the addition of NaBH₄ (2.88 mL; 0.1 M). The resulting colloid (acidified at pH 2 by sulphuric acid) was immobilized by adding carbon (1.4 g) under vigorous stirring in order to have a final metal loading of 1 wt% (0.608 mmol%). After 2 h, the slurry was filtered off and the catalyst was thoroughly washed with distilled water to remove residual chlorine present, if any. The catalyst was dried for 5 h at 120 °C and used for characterization and catalytic evaluation. The size effect of the Au nanoparticles with varying particle size were prepared and subsequently supported on activated carbon (AC) by varying the NaAuCl₄ concentration from 5 × 10⁻⁴ to 5 × 10⁻³ M whilst NaBH₄ and PVA are kept constant.

2.5. Characterization

UV-VIS spectra of Au-sols were performed on Jasco V-530. UV-Visible spectrophotometer in H₂O between 200 and 800 nm, in a quartz cuvette with a scan rate of 200 nm per min. Diffraction patterns were recorded using a Bruker D8 Focus Advance diffractometer equipped with LynxEye detec-

tor with a Ni-filtered Cu K α radiation source ($\lambda = 1.5406 \text{ \AA}$) operating at 40 kV and 40 mA. Low (0.5–7°) and high angle (10–80°) diffraction patterns were recorded separately with a scanning rate of 0.5° and 1° min⁻¹ respectively. The crystallite size was calculated by X-ray line broadening using Scherrer method $d = K \lambda / (\beta \cos \theta)$ where, d is the crystallite size in nm, K is the numerical (crystallite shape) constant ($K = 0.89$), λ is the wavelength of radiation used ($\lambda = 1.5405 \text{ \AA}$), β is full width at half maximum (FWHM) in radians and θ is the Bragg diffraction angle in degrees, at the peak maximum. Transmission Electron Microscope (TEM) analysis of the carbon material was performed on Philips CM12 Transmission Electron Microscope with EDAX attachment.

Nitrogen adsorption-desorption isotherms were obtained at 77 K on Micrometrics ASAP 2020 Porosimetry system. The specific surface area of the samples were calculated according to the Brunauer-Emmett-Teller (BET) method, and pore size distribution curves were obtained from the analysis of nitrogen desorption isotherms using Barrett-Joyner-Halenda (BJH) method for mesoporous materials and Horvath-Kawazoe (HK) method for microporous AC. FT-IR spectra of various mesoporous silica and carbon samples were recorded on Bruker Tensor 27 FT-IR spectrometer with 4 cm⁻¹ resolution and 100 scans in the mid IR (600–4000 cm⁻¹) region using the KBr pellet technique. FT-Raman spectra of various samples were recorded using Bruker Multi RAM FT-Raman spectrometer attached with a Nd:YAG diode pumped laser (1064 nm) as the excitation source having an output power of 1 W and liquid nitrogen cooled germanium detector.

The gold content in the catalyst was analysed using Inductively Coupled Plasma Optical Emission Spectrometer (ICP-OES, Perkin Elmer Optima Model 5300 DV) after calibration with standard solution containing known metal content. XPS measurements were performed with an Omicron Nanotechnology spectrometer with hemispherical analyzer. The monochromatized Mg K α X-ray source ($E = 1253.6 \text{ eV}$) was operated at 15 kV and 20 mA. For the narrow scans, the analyzer pass energy of 25 eV was applied. The base pressure in the analysis chamber is 5 × 10⁻¹⁰ torr.

2.6. Catalytic Evaluation

All the prepared catalysts were tested for glycerol oxidation reaction. Glycerol, NaOH (glycerol/NaOH = 4 mol/mol) and the supported nano-gold catalyst (glycerol/metal = 500 mol/mol) were dispersed in 10 mL of distilled water and kept in autoclave (Parr, 100 mL). Initially, the reactor was pressurized with 7 bar O₂ and thermostated at the 60 °C. After the reaction mixture was allowed for 5 h the collected products were analysed by HPLC with refractive index (RI) detector. Reactant and products were separated on an ion-exclusion

column (Alltech OA-1000 organic acid) heated at 80 °C with 0.5 mL min⁻¹ of H₂SO₄ (0.0004 M) as the eluent. Products were recognized by comparison with authentic samples. Conversion is defined as the ratio of moles of glycerol converted to moles of glycerol initially charged. Selectivity towards a specific product is given as the ratio of moles of specific product to the total moles of glycerol. Carbon balance is defined as the ratio of moles of carbon in all products to that in the converted glycerol. Conversion, selectivity and carbon balance are expressed in mole percentage. Turnover frequency (TOF) is defined as the number of molecules of glycerol converted per active site per second.

3. Results and Discussion

3.1. OMC

Figure 1 shows the low angle XRD patterns of mesoporous carbon products such as CMK-3, NCCR-56 and those of the ordered mesoporous silica (OMS) templates SBA-15 and IITM-56, respectively. The ordered porous carbons, viz., CMK-3 and NCCR-56, obtained from the silica templates such as SBA-15 and IITM-56, respectively have exhibited well resolved peaks which are typical of highly ordered 2D hexagonal mesoporous structures.^[14–15] An intense reflection representing (100) crystal plane of 2D-hexagonal structure is observed for both silica templates as well as the corresponding mesoporous carbons indicating proper replication of 2D-hexagonal porous structures. The appearances of well defined

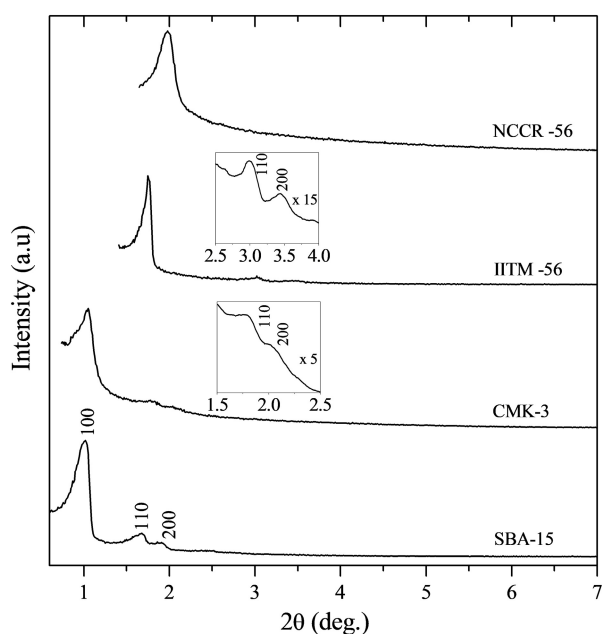


Figure 1. XRD patterns of SBA-15; CMK-3; IITM-56; NCCR-56.

reflections in the diffraction patterns suggest the formation of long-range ordered porous materials. As expected, the main reflections of the carbon replicas were found to systematically shift towards higher-angle in comparison with that of their corresponding silica counterparts, indicating a reduction in the size of the unit cell (Table 1). On the other hand, the broadening of the reflections observed, in particular, for the mesoporous carbons signifies the presence of disordered pore structure as compared to the mesoporous silica structures.

Table 1. Structural and textural properties of OMS and OMC.

Material	a_0^a (nm)	h_w^b (nm)	S_{BET} (m ² g ⁻¹)	V_p (cm ³ g ⁻¹)	D_{BJH} (nm)	D_{TEM} (nm)
SBA-15	10.08	3.58	663	1.10	6.5	6.6
CMK-3	9.77	5.47	1080	1.26	4.3	4.5
Au/CMK-3	9.93	5.73	1032	1.17	4.2	4.3
IITM-56	5.94	2.14	772	1.00	3.8	3.6
NCCR-56	5.10	1.90	1367	1.40	3.2	2.9
Au/NCCR-56	4.88	1.58	1243	1.30	3.3	3.3
AC	—	—	1080	0.80	1.3	—
Au/AC	—	—	1049	0.79	1.4	—

^aAverage unit cell parameter calculated using $1/d^2 = 4/3(b^2 + bk + k^2/a^2)$. ^bWall thickness, $h_w = a_0 - D_{\text{BJH}}$.

The N₂ adsorption-desorption isotherms and pore size distribution of OMSs (SBA-15, IITM-56) and corresponding OMCs (CMK-3, NCCR-56) are shown in Figure 2. The textural parameters of the materials are given in Table 1. Both OMS and OMC exhibited type-IV isotherms with H1 hysteresis loop indicating the mesoporous characteristics. The mean pore size of CMK-3 and NCCR-56 are 4.3 nm and 3.3 nm respectively which are lower than their corresponding silica templates; the distinct, narrow pore-size distribution reveals the retention of mesoporous structure with uniform pores.

Figure 3 depicts the FT-IR spectra of SBA-15 and CMK-3, which reveal signatures of the various functional groups present at the surface of the ordered mesoporous silica and carbon. The stretching and bending mode of O–H are seen as broad signals in the range 3100–3800 cm⁻¹ and at 1633 cm⁻¹ respectively. The signal corresponding to asymmetric and symmetric C–H stretching vibrations of sp²-type carbon are observed at 2985 and 2879 cm⁻¹. On the other hand, the signals related to asymmetric, symmetric C–H stretching and bending vibrations of sp³-type carbon are seen at 2950, 2828 cm⁻¹ and at 1355 cm⁻¹ respectively. The presence of C=C and C–C bonds of aromatic rings is supported by the bands at 1520 and 1410 cm⁻¹, respectively. The broad signal in the range 1150–1300 cm⁻¹ is assigned to C–O stretching and O–H bending modes of alcoholic,

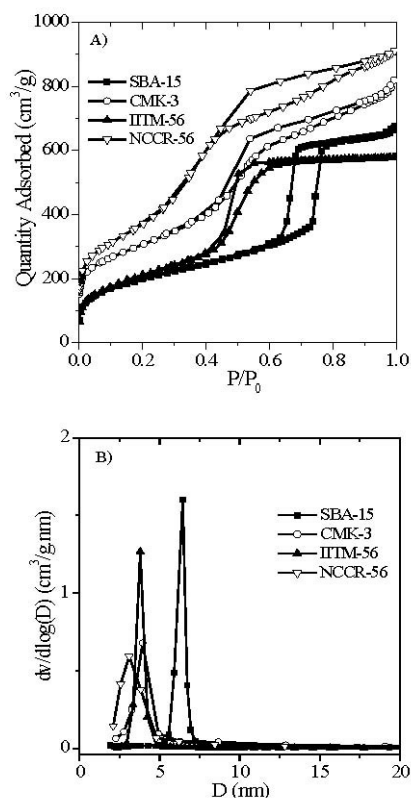


Figure 2. (A) N_2 sorption isotherms and (B) Pore size distribution.

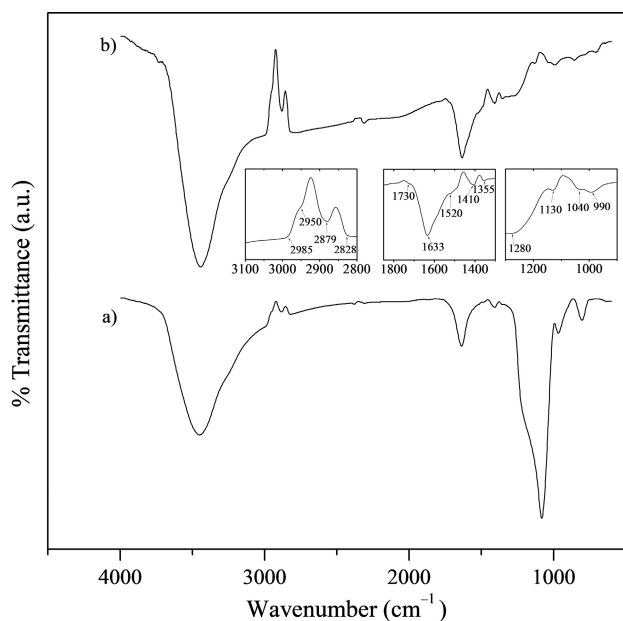


Figure 3. FT-IR spectra of: (a) SBA-15; (b) CMK-3. Insets: corresponding functional groups of CMK-3.

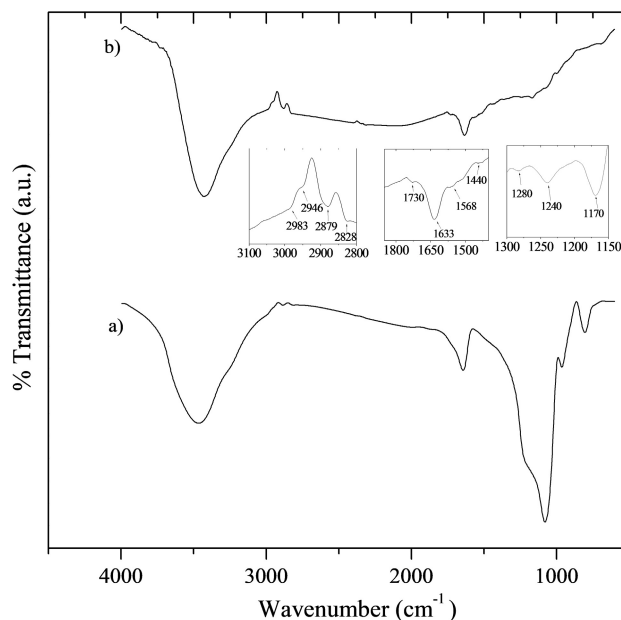


Figure 4. FT-IR spectra of: (a) IITM-56; (b) NCCR-56. Insets: corresponding functional groups of NCCR-56.

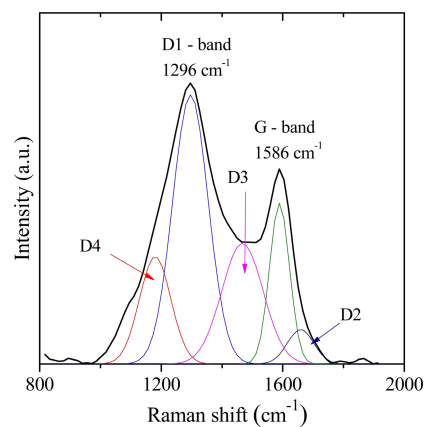


Figure 5. FT-Raman spectrum of CMK-3.

phenolic, and carboxylic groups. Stretching vibration of $C=O$ gives rise to a band at 1730 cm^{-1} . The complete removal of silica from the ordered mesoporous carbons is substantiated by the absence of a band at 1100 cm^{-1} arising due to symmetric vibration of $Si-O-Si$. Similar vibrational characteristics are observed in case of IITM-56 and NCCR-56 and the spectra are shown Figure 4.

Figure 5 shows the FT-Raman spectrum of CMK-3 which exhibits two distinct signals at 1296 cm^{-1} and 1586 cm^{-1} corresponding to D1-band and G-band, respectively. Figure 6 shows the FT-Raman spectrum of NCCR-56, in which two distinct signals at 1287 cm^{-1} and 1587 cm^{-1} corresponding to

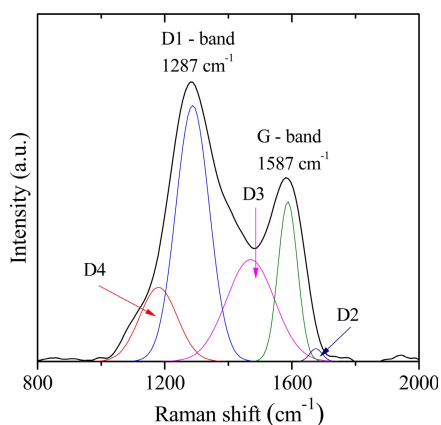


Figure 6. FT-Raman spectrum of NCCR-56.

D1-band and G-band, respectively are observed. The presence of broad D1-band corresponding to a graphitic lattice vibration mode with A_{1g} symmetry in the spectra indicate the possible disordered arrangement of carbon in the pore walls leading to the loss of hexagonal symmetry of the graphitic framework structure.^[17] Furthermore the D2 band for both the carbons corresponds to a defective graphitic lattice mode with E_{2g} symmetry. The intensity of G band is more in case of CMK-3 sample; So it is expected that the intensity of D2 band will be more intense in case of CMK-3 sample. The prominent D3 band at around 1470 cm^{-1} originates from the amorphous carbon fraction contributed largely by the walls of mesoporous carbon CMK-3 and NCCR-56. The band at $\sim 1180\text{ cm}^{-1}$ in Raman spectra of both the mesoporous CMK-3 and NCCR-56 carbon could be attributed to diamond like carbons with significant fraction of sp^3 bonds.

On the other hand, the relative integrated area of the D1-band and G-band (A_{D1}/A_G) of CMK-3 is 2.97 and NCCR-56 is 2.73, indicating that the mesoporous carbon is composed of folded graphene sheets with a small degree of graphitization and high degree of disordered surface.^[18] Further, the integrated peak intensity ratio of the D- and G-bands is used to quantify the changes in-plane crystallite sizes (L_a) which is 128 nm and 146.4 nm respectively for CMK-3 and NCCR-56.

XPS is a surface technique which provides valuable information on the chemical composition, electronic state and oxidation state of the elements that exist in the few uppermost layers of the surface.^[19] C (1s) XPS spectrum of CMK-3 (Figure 7) features an intense peak at 284.4 eV which could be attributed to both amorphous/disordered (diamond-like) and graphitic carbons, in agreement with FT-IR data, the bands (deconvoluted) at 286.0 , 287.2 and 288.8 eV are attributed to the presence of oxygen-containing functional

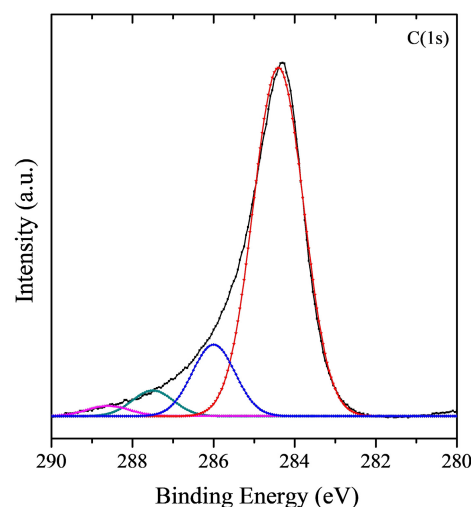


Figure 7. XP spectrum of CMK-3.

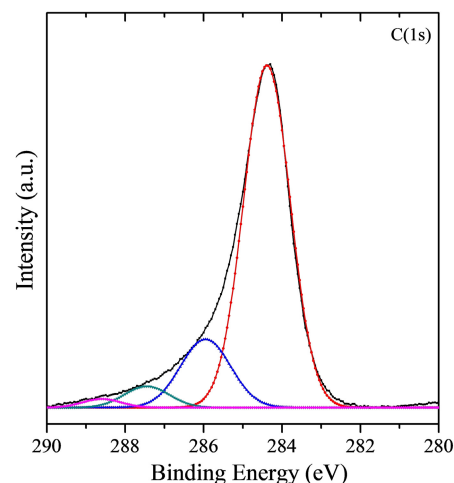


Figure 8. XP spectrum of NCCR-56.

groups such as C–OH, C=O and COOH, respectively.^[20] Similar observations are made in case of NCCR-56 and spectrum is presented in Figure 8.

3.2. Catalytic Stability of Au/OMC

The surface area of OMC samples has been slightly decreased after Au loading because the Au nanoparticles are within the pores of OMCs (*see* Table 1). The XRD patterns of Au/OMC and regenerated (second cycle) catalysts after the catalytic reaction are shown in the Figure 9 and 10. A strong reflection of (111) plane corresponding to face-centered cubic (FCC) lattice of gold was observed for all gold nanoparticles immobilized on carbon. However the broad features of (111) plane reveals that the Au metallic clusters are of nano-size and

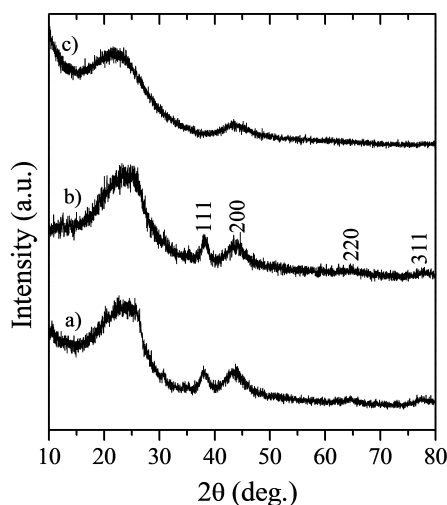


Figure 9. XRD patterns of: (a) Au/CMK-3 (fresh), (b) Au/CMK-3 (recycled), and (c) CMK-3.

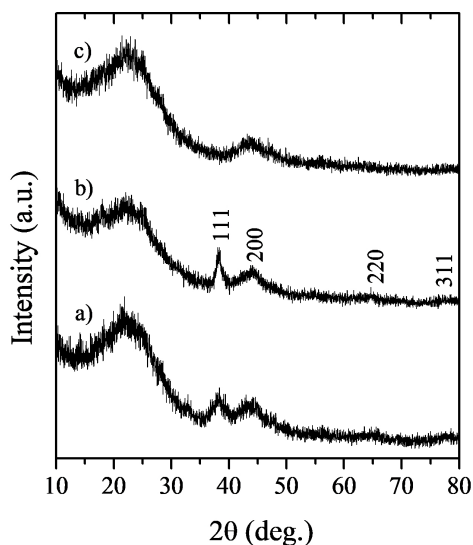


Figure 10. XRD patterns of: (a) Au/NCCR-56 (fresh), (b) Au/NCCR-56 (recycled), and (c) NCCR-56.

possibly well dispersed over the carbon support. The crystallite sizes are calculated by using the Scherrer equation and they are well correlated with TEM data which is given in Table 3. In the case of Au/CMK-3 and Au/NCCR-56 catalyst the intensity of the peak corresponding to the plane (111) remained unchanged, even after regeneration (second cycle) which reinstates the presence of monodispersed and uniform gold particles even after the reaction (Figure 9b & 10b).

The corresponding gold loaded carbon samples are shown in Figures 11 and 12. SBA-15 and IITM-56 (Figure 11a and 12a) exhibit well ordered mesoporous channels and the

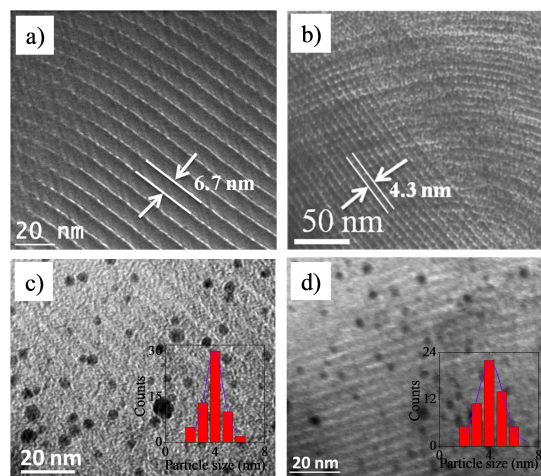


Figure 11. TEM images of: (a) SBA-15; (b) CMK-3; (c) Au/CMK-3; (d) Au/CMK-3 recycled. Inset: Gold particle size distribution.

carbon samples CMK-3 and NCCR-56 (Figure 11b and 12b) reveal that the structures of these mesoporous carbons are exactly inverse replica of their silica counterparts.^[15] Further, the micrographs of Au/CMK-3 and Au/NCCR-56 sample (Figure 11c and 12c) reveal an excellent dispersion of gold nanoparticles with a narrow particle size distribution which is ably supported by the histogram (inset). These micrographs clearly illustrate the uniform grafting of Au particles onto the mesoporous channels of carbon supports. In case of Au/CMK-3 and Au/NCCR-56 catalysts, the particle size remained significantly unchanged even after regeneration (second cycle) which demonstrates the role of mesoporous network in preventing the aggregation of gold nanoparticles during the reaction (Figure 11d and 12d).

The surface oxidation states of the Au nanoparticles dispersed over the carbon support is determined by XPS.^[21] XP spectrum of Au supported CMK-3 in 4f region is shown in the Figure 13. The gold nanoparticles grafted over the mesoporous carbon supports gave rise to peaks at a binding energy of 83.9 and 87.6 eV corresponding to Au 4f_{7/2} and the Au 4f_{5/2} electrons respectively. The intense component of the deconvoluted signal of Au 4f_{7/2}, observed at 83.9 eV is attributed to metallic (Au⁰) whereas the component at 85.0 eV is due to non-metallic gold (Au⁺) and a weak signal at 86.5 eV represents the presence of Au⁺³. Similar trend has been observed for Au 4f_{5/2} signal as the peak component at 87.6 eV is due to metallic Au⁰ whereas the component at 88.7 eV and a weak signal at 90.2 eV are attributed to non-metallic (Au⁺) and Au⁺³ respectively. The electronic characteristics of Au/NCCR-56 resembled as that of Au/CMK-3 and the spectrum is given in Figure 14. But from the area of the deconvolution peaks (Table S3) we have observed that

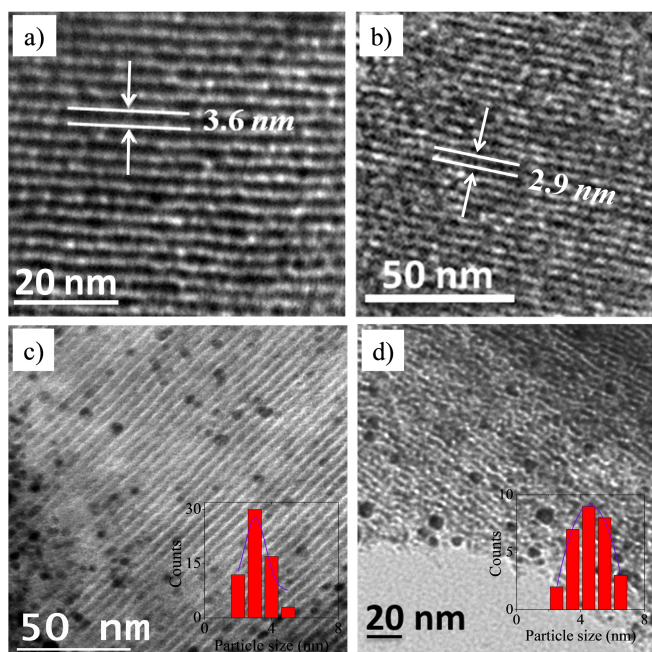


Figure 12. TEM images of: (a) IITM-56; (b) NCCR-56; (c) Au/NCCR-56; (d) Au/NCCR-56 recycled. Inset: Gold nanoparticles size distribution.

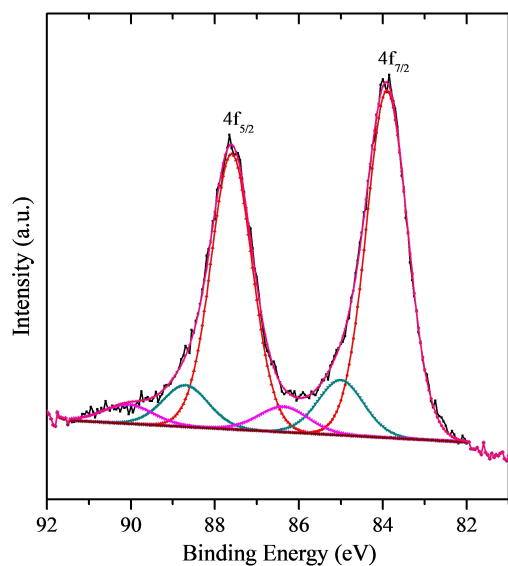


Figure 13. XP spectrum of Au/CMK-3.

more amount of gold present on the surface of Au/NCCR-56 catalysts than on Au/CMK-3.

3.3. Catalytic Instability of Au/AC

As shown in Table 2, the Au absorption bands of all samples shifted from 511 to 532 nm suggesting that the monotonically

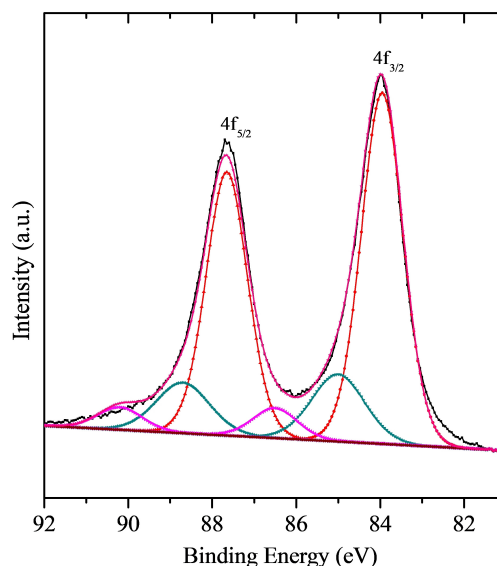


Figure 14. XP spectrum of Au/NCCR-56.

Table 2. Structural and spectral properties of Au/AC.

Catalyst ^a	Structural data Au/ <i>a</i> ₀ (nm) ^b	Particle size (nm)		UV-VIS λ_{max} (nm) ^c
		XRD	TEM	
5×10^{-4} M	0.4082	4.5	4.1 ± 1.1	511
6×10^{-4} M	0.4074	6.7	7.0 ± 1.6	515
1×10^{-3} M	0.4072	8.8	8.9 ± 2.6	520
3×10^{-3} M	0.4069	10.9	11.1 ± 3.0	526
5×10^{-3} M	0.4068	12.8	13.0 ± 5.0	532

^a1 wt% Au/AC prepared using various concentration of gold sol;

^b $a = d \times (h^2 + l^2 + k^2)^{1/2}$; ^cAu-sol.

increase with the particle size as a function of the precursor concentration. Figure 15 depicts XRD patterns of various AC supported gold catalysts. All the samples exhibit typical reflections corresponding to the gold nanoparticles present on the AC support. The characteristic reflections corresponding to FCC gold clearly indicate the quality of the samples. However, the broad features reveal that the metallic gold clusters are of nano-size and possibly dispersed well over the carbon-support. The size of particles were calculated using the Scherrer equation by considering the full width at half maximum of the intense (111) reflection, and agree reasonably well with the particle size values obtained from TEM (see Figure 16).

Figure 16 illustrates the TEM bright field images of Au-NSP and Au/AC samples. It can be seen from these images that good dispersion of gold nanoparticles with a narrow particle size distribution is achieved. The average crystallite size obtained by TEM is in close agreement with the values calculated from the XRD data (Table 2). The selected area

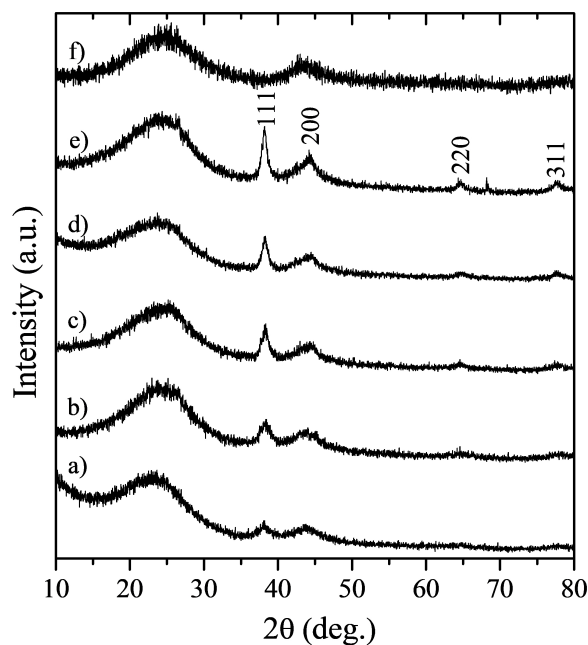


Figure 15. XRD patterns of 1 wt% Au/AC catalyst prepared using different NaAuCl_4 concentration (M): (a) 5×10^{-4} ; (b) 6×10^{-4} ; (c) 1×10^{-3} ; (d) 3×10^{-3} ; (e) 5×10^{-3} ; (f) AC.

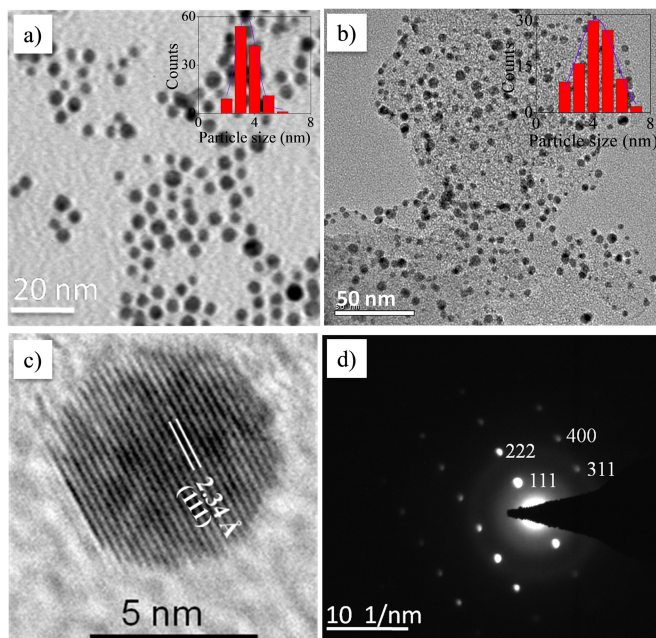


Figure 16. TEM image of: (a) Au-NSP, 5×10^{-4} M NaAuCl_4 ; (b) Au/AC; (c) single Au particle; (d) SAED of Au. Inset: gold particle size distribution.

electron diffraction pattern shown in Figure 16d also confirms the highly (single) crystalline nature of the gold with lattice constant of ~ 0.4 nm.

Stability studies: TEM images of Au-NSP before and after the reaction were shown in Figure 17. It can be seen from this figure that before the reaction, the gold-sol comprises of uniform nanoparticles while, after reaction, they get agglomerated. Figure 18 shows UV-VIS spectra of Au-NSP recorded before and after the reaction. It can be seen from this figure that the SPR band is red-shifted for the used sample, *i.e.*, the band appear at 557 nm as against 511 nm for the fresh sample. It is, therefore, clear that the nanoparticles agglomerated during the glycerol oxidation reaction in agreement with TEM images (*cf.* Figure 17).

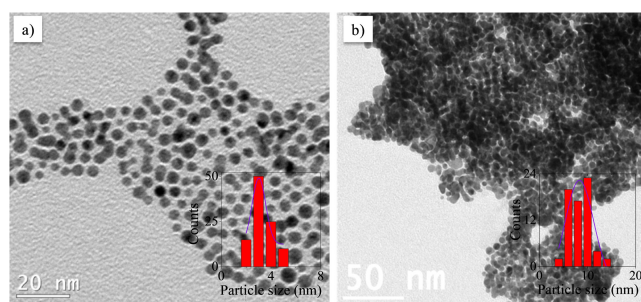


Figure 17. TEM images of Au-NSP: (a) Before reaction; (b) After reaction. Inset: particle size distribution.

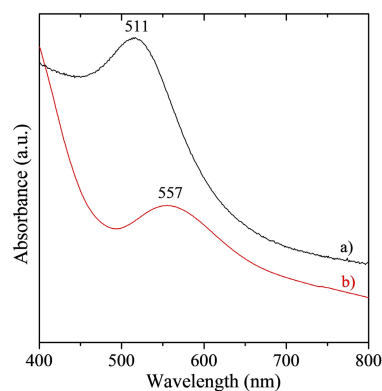


Figure 18. UV-VIS spectra of Au-NSP: (a) Before; (b) After reaction.

A similar observation can also be noticed for the Activated carbon-supported samples. For example, the diffraction pattern of regenerated catalyst, *viz.*, Au/AC (Figure 19b), shows sharper reflection indicating increased size of the gold (*see also* Table 3). This is well supported by TEM micrographs (Figure 20b), *i.e.*, fresh catalyst shows excellent dispersion with a narrow particle size distribution while the regenerated catalyst shows larger sizes due to agglomeration.

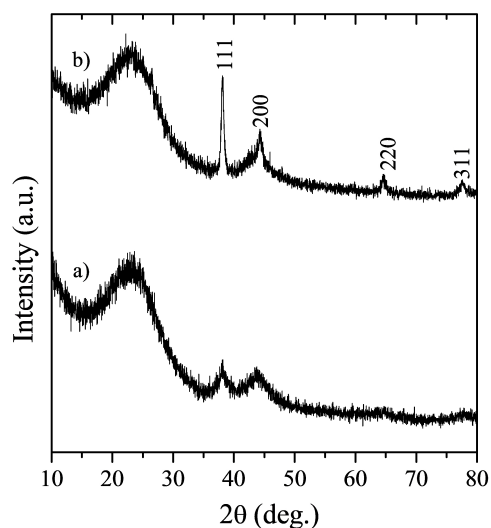


Figure 19. XRD patterns of Au/AC: (a) Fresh; (b) Recycled.

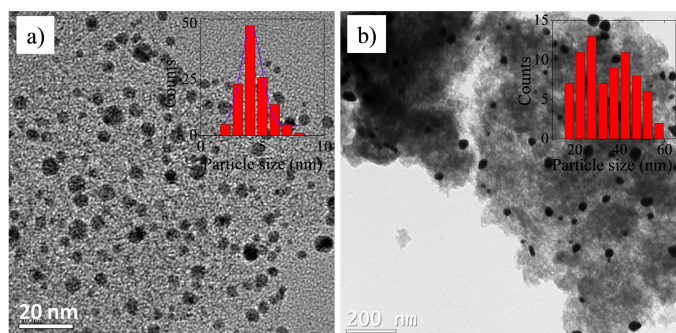


Figure 20. TEM images of Au/AC: (a) Fresh; (b) Recycled. Inset: particle size distribution.

3.4. Catalytic Activity

Size-dependent activity: The oxidation of glycerol was carried out over AC-supported gold nanoparticles with varied sizes. In this reaction, glyceric acid was obtained as major product along with by-products such as glycolic acid, tartronic acid and oxalic acid. The effect of gold nanoparticle size on the glycerol conversion and selectivity of the glyceric acid product is illustrated in Figure 21. The impact of the size on the reactivity can clearly be noticed and that it can also be observed that upon increasing the size of the gold particle size, the glycerol conversion monotonically decreases and that glyceric acid selectivity remain nearly constant. The former could be attributed to the reduction in the surface active gold, i.e., with an increase in size, the surface-to-volume ratio decreases and therefore the lower activity.

Regeneration studies: The catalytic activities of OMC and AC supported Au catalysts are tested for the glycerol oxidation and the results are presented in Table 3. During the reaction along with the glyceric acid which is the desired product, other oxidation products such as tartronic acid, glycolic acid and oxalic acid are also formed. The porous nature of the support also influence the selectivity of glyceric acid according to the report of Rodrigues et al.^[22] and that these liquid products accounted for majority of the carbon balance (93%) for reactions with Au/CMK-3 and Au/NCCCR-56 catalysts. CO₂ might be the gaseous product formed (not identified in the present case) during the reaction according to the reports of Liu et al.^[23] and Zhao et al.^[24] The carbon balance noted in the present work is agreement with that observed for the oxidation of glycerol using gold catalyst.^[25]

All the mesoporous carbon supported Au catalysts exhibit an excellent performance under similar reaction conditions and exhibited higher TOF when compared to that supported on AC. The regenerated catalysts (second cycle) of OMCs

Table 3. Catalytic activity of carbon-supported nano-gold.^a

Catalyst	<i>d</i> (nm)		Au ^b (wt %)	X (mol %)	Selectivity (mol %)					TOF ^c (h ⁻¹)	Carbon balance (mol %)
	XRD	TEM			A	B	C	D	E		
Au/CMK-3											
Fresh	4.2	3.9 ± 1.3	0.52	82	71	8	15	5	1	96	92.9
Recycled	4.8	4.1 ± 1.3	–	84	70	10	14	6	–	–	92.8
Au/NCCCR-56											
Fresh	3.2	3.1 ± 0.9	0.52	84	70	7	17	4	2	99	93.3
Recycled	5.3	5.1 ± 1.8	–	84	71	6	16	5	2	–	93.2
Au/AC											
Fresh	4.5	4.1 ± 1.1	0.58	88	72	7	13	7	1	92	93.3
Recycled	23.0	35 ± 11	–	48	76	3	11	10	–	–	93.0

^aReaction conditions: Glycerol = 0.3 M; glycerol/Au = 500 mol/mol; glycerol/NaOH = 4 mol/mol; water = 10 mL; T = 60 °C; pO₂ = 7 atm; t = 5 h. ^bICP-OES data. ^cTOF calculated by using TEM results. X = Glycerol conversion; A – Glyceric acid; B – Tartronic acid; C – Glycolic acid; D – Oxalic acid; E = Others.

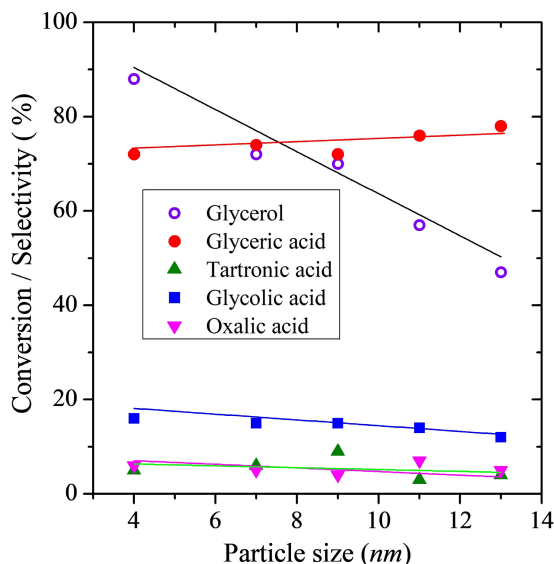


Figure 21. Effect of the size of gold nanospheres on the oxidation of glycerol over Au/AC catalysts. Reaction conditions: Glycerol = 0.3 M, glycerol/Au = 500 mol/mol, glycerol/NaOH = 4 mol/mol, water = 10 mL, T = 60 °C, $pO_2 = 7$ atm, $t = 5$ h.

supported Au Nanoparticles (Au/CMK-3 and Au/NCCR-56) show similar activities as that of fresh catalysts and the carbon balance remained high for the recycled catalyst as well. This remarkable catalytic activity as well as selectivity (towards glyceric acid) of the regenerated catalysts (second cycle) is ascribed to the textural integrity of the catalysts. As it is inferred from XRD and TEM analyses the non-agglomeration of gold nanoparticles over the mesoporous support during the high pressure reaction demonstrates the hydrothermal stability of the OMC supported catalysts, due to the presence of pore channels in mesoporous carbons which act as nanoreactors and thus prevent the agglomeration of nanoparticles. On the other hand, activity of AC supported Au is dropped significantly where the disordered amorphous carbon failed to restrict the agglomeration of gold nanoparticles.

4. Conclusion

High quality ordered mesoporous carbons, viz., CMK-3 and NCCR-56, were successfully synthesized using SBA-15 and IITM-56 as templates, respectively. The resulting nanostructured carbons, i. e., CMK-3 and NCCR-56, were used as ordered porous carbon supports in order to obtain uniform monodispersed gold nanocatalysts such as Au/CMK-3, Au/NCCR-56. These carbon supported nano-gold catalysts were tested for the oxidation of glycerol. The remarkable performance of both fresh and regenerated catalysts, viz., the mesoporous carbon supported nano-gold catalysts, is attrib-

uted to the key role of ordered porous structure of carbons in maintaining the dispersion of nanoparticles by enclosing them well within the pores. The study further reiterates the importance of ordered pore structure in the supported catalysts systems, in particular, for a favorable mass transfer of reactants and products.

Acknowledgements

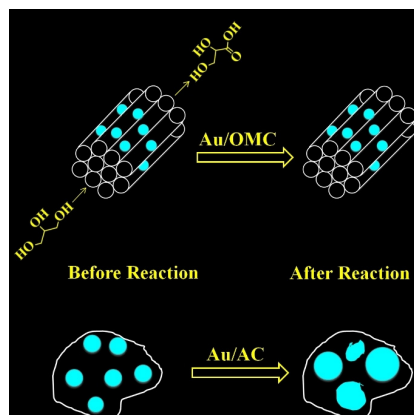
The authors thank Department of Science and Technology (DST), New Delhi for funding NCCR, IIT-Madras. We are also grateful to Professor B. Viswanathan for kind support and constant encouragement. This work is partially supported by a grant-in-aid for the scientific research by the Ministry of New and Renewable Energy (MNRE) under Grant No. 103/140/2008-NT.

References

- [1] a) G. C. Bond, D. T. Thompson, *Catal. Rev. Sci. Eng.* **1999**, *41*, 319–388; b) G. J. Hutchings, *Catal. Today* **2005**, *100*, 55–61; c) M. Haruta, *Faraday Discuss.* **2011**, *152*, 11–32.
- [2] A. Villa, N. Dimitratos, C. E. Chan-Thaw, C. Hammond, L. Prati, G. J. Hutchings, *Acc. Chem. Res.* **2015**, *48*, 1403–1412.
- [3] L. C. Meher, D. Vidya Sagar, S. N. Naik, *Renewable Sustainable Energy Rev.* **2006**, *10*, 248–268.
- [4] a) M. Pagliaro, R. Ciriminna, H. Kimura, M. Rossi, C. Della Pina, *Angew. Chem. Int. Ed.* **2007**, *46*, 4434–4440; *Angew. Chem.* **2007**, *119*, 4516–4522; b) C.-H. Zhou, J. N. Beltramini, Y.-X. Fan, G. Q. Lu, *Chem. Soc. Rev.* **2008**, *37*, 527–549; c) Y. Zheng, X. Chen, Y. Shen, *Chem. Rev.* **2008**, *108*.
- [5] H. Habe, T. Fukuoka, D. Kitamoto, K. Sakaki, *Appl. Microbiol. Biotechnol.* **2009**, *84*, 445–452.
- [6] S. Carretin, P. McMorn, P. Johnston, K. Griffin, C. J. Kiely, G. J. Hutchings, *Phys. Chem. Chem. Phys.* **2003**, *5*, 1329–1336.
- [7] a) L. Wang, Z. Tang, X. Liu, W. Niu, K. Zhou, H. Yang, W. Zhou, L. Li, S. Chen, *RSC Adv.* **2015**, *5*, 103421–103427; b) M. Turner, V. B. Golovko, O. P. H. Vaughan, P. Abdulkhin, A. Berenguer-Murcia, M. S. Tikhov, B. F. G. Johnson, R. M. Lambert, *Nature* **2008**, *454*, 981–983.
- [8] a) L. Prati, A. Villa, A. R. Lupini, G. M. Veith, *Phys. Chem. Chem. Phys.* **2012**, *14*, 2969–2978; b) N. Zheng, G. D. Stucky, *J. Am. Chem. Soc.* **2006**, *128*, 14278–14280; c) P. R. Murthy, A. Aalagarasi, B. Viswanathan, P. Selvam, *Faraday Discuss.* **2011**, p.23.
- [9] N. Dimitratos, A. Villa, C. L. Bianchi, L. Prati, M. Makkee, *Appl. Catal. A* **2006**, *311*, 185–192.
- [10] a) E. Ramasamy, J. Chun, J. Lee, *Carbon* **2010**, *48*, 4563–4565; b) R. Ryoo, S. H. Joo, S. Jun, *J. Phys. Chem. B* **1999**, *103*, 7743–7746.
- [11] a) P. Selvam, B. Kuppan, *Catal. Today* **2012**, *198*, 85–91; b) S. H. Joo, S. J. Choi, I. Oh, J. Kwak, Z. Liu, O. Terasaki,

PERSONAL ACCOUNT

High quality ordered mesoporous carbons such as CMK-3 and NCCR-56 were successfully synthesized and characterized. These materials were used as supports for gold nano-particles and confined inside the pores with narrow size distribution. Their high catalytic stability on activity has been tested for the selective (liquid-phase) oxidation of glycerol.



*Dr. P. R. Murthy, Prof. Dr. P. Selvam**

1 – 14

The Enhanced Catalytic Performance and Stability of Ordered Mesoporous Carbon Supported Nano-gold with High Structural Integrity for Glycerol Oxidation